Near-term forecasts of stream temperature using process-guided deep learning and data assimilation

Jacob Zwart[1], Samantha Oliver[1], David Watkins[1], Jeffrey Sadler[1], Alison Appling[1], Hayley Corson-Dosch[1], Xiaowei Jia[2], Vipin Kumar[3], Jordan Read[1]

[1]U.S. Geological Survey, Water Mission Area

[2]University of Pittsburgh, Department of Computer Science

[3]University of Minnesota, Department of Computer Science and Engineering

Corresponding author: Jacob Zwart (jzwart@usgs.gov)

Abstract

Near-term forecasts of environmental outcomes can inform real-time decision making. Data assimilation modeling techniques can be used for forecasts to leverage real-time data streams, where the difference between model predictions and observations can be used to adjust the model to make better predictions tomorrow. In this use case, we developed a process-guided deep learning and data assimilation approach to make 7-day forecasts of daily maximum water temperature in the Delaware River Basin. Our modeling system produced forecasts of daily maximum stream temperature with an average root mean squared error (RMSE) from 1.2 to 1.6°C for 1-day lead time across all sites. The data assimilation algorithm successfully adjusted the process-guided deep learning model states and marginally improved forecast performance when compared to forecasts produced using the process-guided deep learning model alone (7-13% lower RMSE with the data assimilation algorithm). Our model characterized forecast uncertainty relatively well as 57-80% of observations were within 90% forecast confidence intervals across all sites and lead times, and the uncertainty associated with our forecasts allow managers to anticipate probability of exceedances of ecologically relevant thresholds and aid in decisions about releasing reservoir water downstream. The flexibility of deep learning models to be applied to various prediction problems shows promise for using these types of models to forecast many other important environmental variables and aid in decision making.

Introduction

The intersection between human and environmental water needs can generate complex water allocation decisions that must be made with imperfect information about the future (Vörösmarty et al. 2000). Forecasts are predicted future conditions with associated uncertainty (Clark et al. 2001), and aquatic forecasts are becoming critical management tools for balancing various uses of water to generate more desirable outcomes (Viel et al. 2016; Turner et al. 2020). Parallel advances in predictive modeling, real-time environmental observing systems, and decision analysis tools can be leveraged to create more useful forecast products for water resources decisions.

To date, forecasts of aquatic systems have mostly relied on process-based models and statistical models. These models have enabled managers and stakeholders to anticipate future changes in water temperatures (Thomas et al. 2021), dissolved oxygen concentrations (Matos and de Sousa 1996; Abdi et al. 2020), and streamflow (Block et al. 2009; Hansen et al., 2009; Turner et al. 2020). Process-based models define relations between driver data and the variable being forecasted *a priori*, while statistical models discover relations between driver data and the target variable during a model training phase assuming a few simple assumptions about model structure and distributions. Process error can be a large source of near-term ecological forecast error for process-based and statistical models (Dietze 2017; Massoud et al. 2018; Thomas et al. 2021). This indicates that these types of models may be misrepresenting system dynamics by using rigid equations that simplify the natural world, require *a priori* parameterization, and cannot adapt on the fly to mismatches between predictions and observations.

Deep learning (DL) models, in contrast to process-based and simple statistical models, learn a complex mapping relation between drivers and output by exposing models to training data and an optimization scheme (Shen 2018). DL models can be very accurate and have the potential to reduce error in forecasting by reducing process error. Promising examples of DL-based aquatic forecasting efforts include a short-term forecast of water demand using an artificial neural network by Jain et al. (2001), an accurate DL approach to streamflow forecasting by Xiang and Demir (2020), and algal bloom prediction by Lee and Lee (2018). However, none of these examples have assimilated real-time water observations – such as those available for many sites in the United States (Hirsch and Fisher 2014) – to increase DL prediction accuracy. Data assimilation (DA; Reichle 2008) is commonly used to improve process-based model performance (Thomas et al. 2021), and a DL architecture with a similar ability to update model states with information from real-time data could provide superior forecasts for water-use decisions.

In this paper, we describe a real-time forecasting system of stream water temperature that assimilates observations into a DL model as they are collected and produces forecasts of stream temperature 7 days into the future. We evaluated forecasts issued across 93 consecutive days and assess how the DL forecast performance compares with and without data assimilation and compare this performance to a baseline persistence forecast. These forecasts of stream temperature can be used by resource managers in the Delaware River Basin to optimize releases of water from reservoirs to cool downstream segments while retaining enough water to supply New York City and other municipalities with drinking water.

Methods

Study site

We generated real-time forecasts of stream water temperature in the Delaware River Basin in support of drinking water reservoir management decisions. The Delaware River Basin is an ecologically diverse region and a societally important watershed along the East Coast of the United States as it provides drinking water to over 15 million people (Williamson et al. 2015). The extensive and expanding environmental monitoring network in the Delaware River Basin provides a great opportunity to leverage both historical and real-time aquatic information for forecasting stream water temperature at specific locations or basin wide.

Drinking water reservoirs in the Delaware River Basin provide essential services to the public while also potentially maintaining suitable aquatic habitat in stream segments directly downstream from the reservoirs. The Flexible Flow Management Program between the State of Delaware, the State of New Jersey, the State of New York, the Commonwealth of Pennsylvania, and the City of New York dictates water management in the basin. The 2017 agreement includes provisions that aim to maintain maximum daily stream water temperature below 23.9°C (75°F) in the upper Delaware River Basin (above Lordville, New York) to ensure cold-water stream habitat. The Cannonsville, Pepacton, and Neversink Reservoirs thermally stratify, which means that during the summer, the deep water release points of the reservoirs discharge cold hypolimnetic reservoir water downstream. Reservoir releases can therefore be used to mitigate anticipated temperature exceedances in streams below the dams. Water in the reservoirs is highly regulated given competing demands of drinking water diversions, maintaining flows for habitat and ensuring freshwater at drinking water intakes, and maintaining cold-water stream habitat. The volume of water in the reservoir used to cool downstream river segments ("thermal banks") is therefore limited in volume, and reservoir managers need to anticipate when these downstream segments may exceed thermal thresholds in order to use the thermal banks only when needed. Near-term forecasts of stream water temperature with associated uncertainty can help inform managers of when stream temperature may exceed these thermal thresholds.

There are five sites below three New York City reservoirs that are relevant to release decisions for mitigating temperature exceedances and for which we forecasted water temperature (Figure 1). These sites included two sites on the West Branch of the Delaware River that are affected by releases from the Cannonsville Reservoir (at Hancock, New York and Hale Eddy, New York), one site on the East Branch of the Delaware River that is impacted by releases from the Pepacton Reservoir (at Harvard, New York), one site on the Delaware River (at Lordville, New York) that is affected by releases from both Cannonsville and

Pepacton Reservoirs, and one site on the Neversink River (at Bridgeville, New York) that is affected by releases from the Neversink Reservoir.

Figure 1. *Map of the target water temperature forecasting sites in the Delaware River Basin, with call-outs detailing stream distances between upstream reservoirs (open circles) and target sites (closed circles).*

Datasets

***Table 1**. Summary of the different datasets used to train the deep learning (DL) models and forecast stream temperature 7 days into the future. The DL models produced forecasts with and without data assimilation (DA), and their model performance was compared to a baseline persistence model that only utilized daily maximum water temperature to make forecasts. Dataset sources include the U.S. Geological Survey's National Water Information System (NWIS), the Water Quality Portal (WQP), Spatial Hydro-Ecological Decision System (EcoSHEDS), New York City Department of Environmental Protection (NYCDEP), the Office of the Delaware River Master (ODRM), gridMET, National Oceanic and Atmospheric Administration's Global Ensemble Forecasting System (GEFS), Precipitation Runoff Modeling System with a coupled Stream Temperature Network Model (PRMS-SNTemp), and the General Lake Model (GLM).*

Input category	**Input**	**Source**	**Deep Learning Model**				**Persistence Model**
			Pretraining	*Training*	*Forecasting* DL	DL+DA	*Forecasting*
Observations	Aggregated daily maximum stream temperature	NWIS, WQP, EcoSHEDS		●	●	●	●
	Daily average reservoir release volume	NWIS, NYCDEP	●	●			
	Reservoir releases on forecast issue date	NWIS			●	●	
Scenarios	Reservoir release scenarios for days 1-7	ODRM			●	●	
Gridded weather drivers	Daily minimum air temperature	gridMET	●	●			
		GEFS			●	●	
	Daily maximum air temperature	gridMET	●	●			
		GEFS			●	●	
	Solar radiation	gridMET	●	●			
		GEFS			●	●	
Modeled stream temperature	Process-based average daily stream temperature predictions	PRMS-SNTemp, GLM	●				

To train our models and forecast stream water temperature at these sites, we pulled publicly available datasets from the U.S. Geological Survey's (USGS) National Water Information System (NWIS) (USGS 2021), the Water Quality Portal (WQP; Read et al. 2017), Spatial Hydro-Ecological Decision System (EcoSHEDS, http://db.ecosheds.org/), gridMET (Abatzoglou 2013), and the National Oceanic and Atmospheric Administration's Global Ensemble Forecasting System (GEFS, https://nomads.ncep.noaa.gov/). We also pre-trained our DL models on process-based model output in order to guide the model towards more physically consistent predictions of water temperature (as in Jia et al. 2021). Below we briefly describe the training and forecasting datasets used to make near-term future predictions of stream temperature.

Spatial fabric and stream temperature observation dataset

We used the National Geospatial Fabric to define our stream segment physical characteristics, including segment length and location (Bock and Viger 2014; Viger 2014). We pulled sub-daily observations of stream water temperature from NWIS, WQP, and EcoSHEDS for both the training dataset and for assimilating in real-time when making forecasts. The sub-daily observations of stream temperature were aggregated to daily maximum temperature values for each site that were used as the target variable for our DL models. We matched observations of maximum stream temperature collected at specific latitude and longitude to the river segments by snapping observations to the nearest stream segment within a tolerance of 250 m. Observations farther than 5,000 m along the river channel to the outlet of a segment were omitted from our training and forecasting dataset. If a site was closer to the upstream segment endpoint than the matched segment endpoint, the upstream segment was used as the location of the observation. Segments with multiple observation sites were aggregated to a single maximum water temperature value.

Historical driver dataset

We used five drivers (i.e. input features) to train our DL models from 1985 to 2021, including gridMET daily minimum and maximum air temperature, daily average downward shortwave radiation, daily average reservoir release volume from the reservoirs directly upstream of each site, and observations of yesterday's maximum stream temperature. When observations of yesterday's maximum stream temperature were not available, we used yesterday's predicted average stream temperature from the process model pre-training dataset (described below). Observations of daily maximum water temperature were available for 68-98% of the training period time steps depending on the stream segment.

Process model pre-training dataset

We used process-based model output from 1985 to 2020 to pre-train the DL models before fine-tuning on observations of maximum water temperature. Pre-training DL models on process-based model output can improve predictive performance, including for out-of-bounds predictions (Read et al. 2019, Jia et al. 2021). For water temperature prediction, process-based models use an energy budget approach to estimating temperature change. Given the utility of learning these physical rules from an existing model and the emphasis on predicting summertime maximum temperatures (which could be poorly represented or out-of-bounds entirely from the training dataset), pre-training was used to generate initial weights and biases for the Long Short-Term Memory (LSTM) that were then refined via training on actual observations (following Jia et al. 2021). For models trained in the Delaware River Basin, we developed a pre-training dataset that combines outputs from a reservoir-ignorant stream temperature model and a reservoir-only temperature model to predict daily average stream temperature from 1980 to 2020. We started with the Precipitation Runoff Modeling System with a coupled Stream Temperature Network Model (PRMS-SNTemp) to make predictions of daily average stream temperature (Markstrom 2012, Sanders et al. 2017). PRMS-SNTemp is a natural flow model, meaning that it does not represent reservoirs within the stream network. This natural flow assumption routinely produces predictions of summer stream temperature that are biased high for segments downstream from reservoirs.

Improved temperature predictions were generated for water emerging from two major reservoirs in the basin, Cannonsville and Pepacton Reservoirs, using the General Lake Model (GLM v3.1; Hipsey et al. 2019). These GLM models required lake structural information and were driven by daily inflows, outflows, and inflow temperatures. Reservoir hypsographic curves were acquired from Nystrom (2018). Observed daily inflows from major tributaries to each reservoir were obtained from the USGS National Water Information System (USGS 2021) and further modified by a multiplier of 1.8 for Pepacton Reservoir and 1.4 for Cannonsville Reservoir to represent total inflows from both gaged and ungaged tributaries; these multipliers were necessary to achieve long-term water balance among inflows, outflows, precipitation, runoff, and evaporation in each reservoir. Inflow temperatures were estimated as the flow-weighted average of PRMS-SNTemp daily predictions of average stream temperature in the gaged tributaries. Recorded outflows (releases and diversions) were obtained from USGS New York Water Data Reports (USGS 2021). Given these input data, the GLM parameters *cd* (bulk aerodynamic transfer coefficient for momentum), *sw_factor* (scaling factor for shortwave radiation), and *Kw* (light extinction coefficient) were then calibrated to in-reservoir water temperature observations, which were provided by the New York

City Department of Environmental Protection (NYC DEP; Oliver et al. 2021). We used the calibrated GLM models to predict the temperature of released water, computed as the flow-weighted average of reservoir water temperatures at the two release depths (one surface, one deep) for each reservoir.

The pre-training dataset was computed as a weighted average of temperature predictions from PRMS-SNTemp and GLM, where GLM predictions only influenced stream segments downstream from GLM-modeled reservoirs. The weight given to GLM predictions in each reach was a function of distance, where stream segments closer to upstream reservoirs had temperatures more similar to the reservoir releases. The weight began at 1 at the reservoir outlet and declined with distance downstream according to an exponential decay function that was fit to stream temperature observations; the decay rate was 0.036 km^{-1} for Cannonsville Reservoir and 0.040 km^{-1} for Pepacton Reservoir, such that the weight given to GLM predictions was <0.1 after 64 stream kilometers.

Forecasted driver dataset

When making near-term forecasts, we used the National Oceanic and Atmospheric Administration's Global Ensemble Forecast System (GEFS, https://nomads.ncep.noaa.gov/) operational forecasts of minimum and maximum air temperature, and daily average downward shortwave radiation to predict daily maximum stream temperature for the forecast issue date and 7 days into the future. We also used yesterday's maximum temperature and today's reservoir releases as additional drivers (Table 1). We generated predictions one day at a time, building on predictions from days earlier in the prediction sequence. For predictions made with a zero day lead time (i.e. nowcast), we used today's reservoir releases and yesterday's maximum temperature analysis after assimilating observations (see data assimilation section) as drivers. For predictions made with 1-7 day lead times, we used reservoir release scenarios (see release scenario description below) and model predictions of yesterday's maximum temperature as drivers.

We can anticipate realistic release scenarios for 7 days in the future because the Flexible Flow Management Plan dictates release volumes that are mandated given the day of year and current reservoir storage. These releases are referred to as "conservation releases" and are set once per month. For every forecast generated, we made forecasts using two different reservoir release scenarios, one with no additional reservoir release (current conservation release volume +0cfs) and one simulating a relatively high reservoir release scenario (current conservation release volume +100cfs). The +0cfs scenario simulates normal reservoir operations, whereas a +100cfs scenario simulates a thermal bank release that would be used to mitigate expected temperature exceedances. The +100cfs scenario is typically a 20% increase in outflow from the Cannonsville Reservoir. The additional reservoir release scenario was only added on to the lead time day 1 reservoir release driver (Figure 2) and was intended to help the reservoir manager anticipate what would happen to stream temperature tomorrow if a thermal release was made.

We downloaded GEFS V12.0 0.25-degree operational model (https://nomads.ncep.noaa.gov/) output daily and used the 00 UTC (19:00 EDT) forecast cycle when making stream temperature forecasts. The operational GEFS saves valid times at 3-hour intervals, i.e. 00:00, 03:00, etc. in UTC for 240 hours past the forecast issue time. Starting with the 03:00 valid time, timesteps represent the average, minimum, or maximum of the preceding 3 hours depending on the meteorological driver forecasted. To transform these timesteps to daily values in average solar time in the Delaware River Basin (approximately UTC – 5:00), we treat the 09:00 through 30:00 UTC (4:00-25:00 in UTC –5:00) timesteps as day zero, 33:00 – 54:00 UTC (28:00 – 49:00 in UTC – 5:00) as day one, and so on. This provides the closest possible alignment of GEFS timesteps with average solar time in the Delaware River Basin. Minimum, maximum, and average daily values for these timesteps were then calculated for each GEFS grid cell for minimum air temperature, maximum air temperature, and downward shortwave radiation, respectively. To map GEFS values to individual stream segments, we matched a 0.25-degree NOAA GEFS grid cell with the centroid of the target stream segment and used the meteorological drivers of that grid cell for the given segment. All stream segments were almost entirely contained within a single NOAA GEFS grid cell. All 31 ensemble members were used to make ensemble forecasts of stream temperature; see the model forecasts section below for how the GEFS ensembles are incorporated into the DL forecasts.

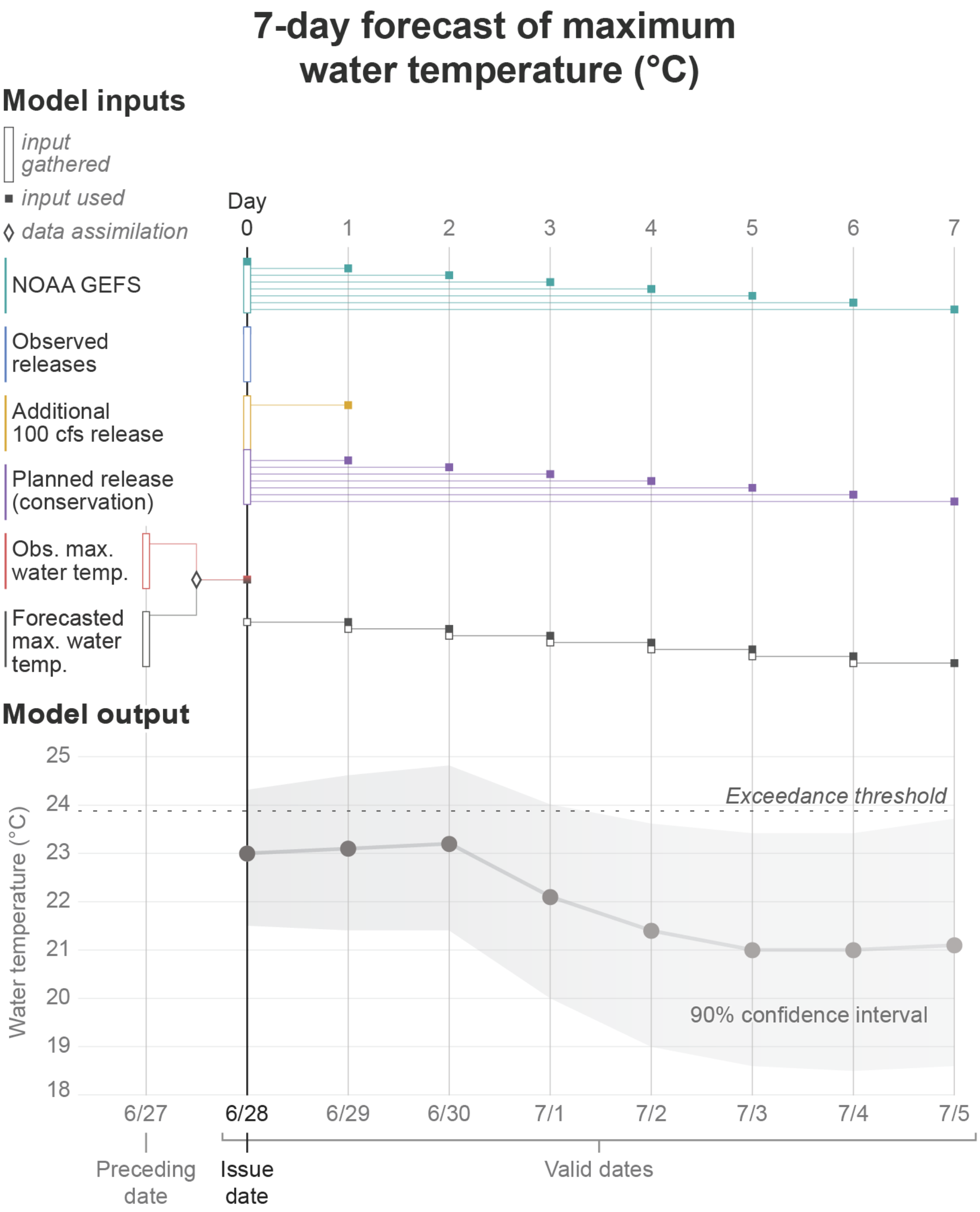

Figure 2. *Schematic of forecast inputs and outputs for the deep learning with data assimilation model, including when observations or driver data are being generated and used in the model. The model output panel shows forecast ensemble averages and 90% confidence interval for the forecast issued on June 28, 2021, for the Delaware River at Lordville site.*

Deep learning model

We used a Long Short-Term Memory (LSTM) network to forecast daily maximum stream temperature. An LSTM is a type of Recurrent Neural Network (RNN) that captures temporal relations between system states and has been used in several other hydrologic modeling applications with great success (Kratzert et al. 2018; Rahmani et al. 2020). The cell states of the system, $\boldsymbol{c_t}$, evolve through time and are modified at each time t by a filtered, transformed version of the model inputs at that time, $\boldsymbol{x_t}$ (e.g. meteorological drivers). The LSTM also inherits information from previous model timesteps through a second set of states (hidden states, $\boldsymbol{h_{t-1}}$) that are a function of c_{t-1}. At each timestep, the LSTM first generates a candidate cell state $\widetilde{c_t}$ as:

$$\widetilde{\boldsymbol{c_t}} = \tanh(\boldsymbol{W_h^c h_{t-1}} + \boldsymbol{W_x^c x_t} + \boldsymbol{b_c}) \tag{1}$$

where $\tanh(\cdot)$ is the hyperbolic tangent function, $\boldsymbol{W_h^c}$ and $\boldsymbol{W_x^c}$ are learnable weight matrices of the hidden state and input features, respectively, and $\boldsymbol{b_c}$ is a learnable bias vector. $\widetilde{\boldsymbol{c_t}}$ represents new 'memories' that could be added at timestep t. Then the LSTM generates a forget gate, $\boldsymbol{f_t}$, an input gate, $\boldsymbol{i_t}$, and an output gate, $\boldsymbol{o_t}$, as:

$$\boldsymbol{f_t} = \sigma\left(\boldsymbol{W_h^f h_{t-1}} + \boldsymbol{W_x^f x_t} + \boldsymbol{b_f}\right) \tag{2}$$

$$\boldsymbol{i_t} = \sigma\left(\boldsymbol{W_h^i h_{t-1}} + \boldsymbol{W_x^i x_t} + \boldsymbol{b_i}\right) \tag{3}$$

$$\boldsymbol{o_t} = \sigma(\boldsymbol{W_h^o h_{t-1}} + \boldsymbol{W_x^o x_t} + \boldsymbol{b_o}) \tag{4}$$

where $\sigma(\cdot)$ is the sigmoid function, and $\boldsymbol{W}$ and $\boldsymbol{b}$ are again matrices and vectors, respectively, of learnable model parameters. The forget gate is used to filter the information inherited from $\boldsymbol{c_{t-1}}$, and the input gate is used to filter the candidate cell state at time t, in essence determining how much old and new memory will be passed to the next timestep. The new cell state, $\boldsymbol{c_t}$, and the hidden representation, $\boldsymbol{h_t}$, are computed as:

$$\boldsymbol{c_t} = \boldsymbol{f_t} \otimes \boldsymbol{c_{t-1}} + \boldsymbol{i_t} \otimes \widetilde{\boldsymbol{c_t}} \tag{5}$$

$$\boldsymbol{h_t} = \boldsymbol{o_t} \otimes \tanh(\boldsymbol{c_t}) \tag{6}$$

where $\otimes$ represents element-wise multiplication. The predicted target variables, $\boldsymbol{\hat{y}_t}$ (in this case just maximum stream temperature), are calculated as:

$$\hat{y}_{\boldsymbol{t}} = \boldsymbol{W_h^y h_t} + \boldsymbol{b_y} \tag{7}$$

During the model training phase, all weights, $\boldsymbol{W}$, and biases, $\boldsymbol{b}$, of the LSTM are optimized via iterative minimization of a loss function, $\mathcal{L}$, via the back-propagation algorithm (Rumelhart et al. 1986). Our loss function was the root mean squared error (RMSE) across all timesteps:

$$\mathcal{L} = RMSE = \sqrt{\frac{1}{T}\sum_{t=1}^{T}(\hat{y}_{\boldsymbol{t}} - \boldsymbol{z_t})^2} \tag{8}$$

where T is the total number of training timesteps and $\boldsymbol{z_t}$ are the observations at time t.

We estimated uncertainty in our DL model predictions using Monte Carlo Dropout (MCD) as described in Gal and Gharhramani (2016), where the model randomly removes a proportion of the network's recurrent and input elements (by setting their weights to 0) during each training iteration or prediction activity. When making many predictions using MCD, this produces an ensemble of LSTM model structures, such that the distribution of their predictions approximates the model uncertainty. We used MCD during training and for an ensemble of predictions; specifics of these procedures, model dimensions, and other model hyperparameters are described in the Model Training section below.

Data assimilation

During the forecasting period, we used data assimilation (DA) to adjust the LSTM states based on recently collected maximum temperature observations. Previous studies have shown promise for data assimilation improving DL model predictions (Brajard et al. 2020, Fang and Shen 2020). Additionally, trained LSTM memory cells can represent dynamic system storages that are similar to our understanding of environmental processes (Kratzert et al. 2019a), indicating that certain LSTM cells states could be updated via model-data fusion techniques under the paradigm of using the LSTM as a “scaffold” to connect across different datasets (Dietze et al. 2013).

We used the ensemble Kalman Filter (EnKF) as our data assimilation algorithm to update maximum stream temperature predictions and the cell states of the LSTM (Evensen 1994). We use the EnKF given the ease of adding multiple sources of uncertainty via the ensemble members including meteorological driver uncertainty (e.g. NOAA GEFS ensembles), model process uncertainty (e.g. MCD), and initial condition uncertainty (e.g. initial LSTM states).

We concatenated LSTM state estimates (stream temperature and cell states) into one vector $\boldsymbol{Y}$, and we used this vector for storing model predictions and updating in the EnKF. The $\boldsymbol{Y}$ vector is propagated through the forecasting period using the trained LSTM weights and biases, the LSTM state estimates, and model drivers. The forecasted $\boldsymbol{Y}$ vector is denoted by $\boldsymbol{Y^f}$:

$$\boldsymbol{Y}^{\boldsymbol{f}}_{\boldsymbol{m},\boldsymbol{t}} = \begin{bmatrix} \hat{y}_{\boldsymbol{m},\boldsymbol{t}} \\ \boldsymbol{c}_{\boldsymbol{m},\boldsymbol{t}} \end{bmatrix} \tag{9}$$

where m indicates the m^{th} ensemble member of the model and the model states are estimated as described in equations 5-7. $\hat{y}_{\boldsymbol{m},\boldsymbol{t}}$ was an *s* by 1 vector where *s* was the number of stream segments in the forecasting period for which stream temperature was predicted, and $\boldsymbol{c}_{m,t}$ was an [*s* x *u*] by 1 vector where *u* was the number of hidden units of the LSTM model. When observations were available at a given time step *t*, the $\mathbf{Y}^{\mathrm{f}}$ vector was updated using the Kalman gain. The updated **Y** vector ($\mathbf{Y}^{\mathbf{u}}$) was expressed as:

$$\boldsymbol{Y}^{\boldsymbol{u}}_{\boldsymbol{m},\boldsymbol{t}} = \boldsymbol{Y}^{\boldsymbol{f}}_{\boldsymbol{m},\boldsymbol{t}} + \boldsymbol{K}_{\boldsymbol{t}}\left(\boldsymbol{z}_{\boldsymbol{t}} - \boldsymbol{H}_{\boldsymbol{t}}\boldsymbol{Y}^{\boldsymbol{f}}_{\boldsymbol{m},\boldsymbol{t}}\right) \tag{10}$$

where m was the ensemble member $(m = 1,2, \dots N_m;\ N_m = 3100)$. $\boldsymbol{z}_t$ was an *s* by 1 vector of observation data from each stream segment being modeled in the forecasting period as $\boldsymbol{z}_{\boldsymbol{t}} = \boldsymbol{z}_{\boldsymbol{t}} + \boldsymbol{\varepsilon}$, where $\boldsymbol{\varepsilon}$ was the observation error randomly drawn from a normal distribution with average of 0 and variance of 0.25°C (see description of observation variance below). $\boldsymbol{H}_t$ was an *s* by [*s* + *s* x *u*] measurement operator matrix with ones when observations of stream temperature $[I(z_t)]$ were available and zeros otherwise. Equation 11 shows what $\boldsymbol{H}_t$ would look like if there were two stream segments, *a* and *b*, and three LSTM hidden units:

$$\boldsymbol{H}_{\boldsymbol{t}} = \begin{bmatrix} I(z_t^a) & 0 & 0 & 0 & 0 & 0 & 0 & 0 \\ 0 & I(z_t^b) & 0 & 0 & 0 & 0 & 0 & 0 \end{bmatrix} \tag{11}$$

$\boldsymbol{K}_t$ was the Kalman gain weighting matrix, expressed as:

$$\boldsymbol{K}_{\boldsymbol{t}} = \frac{1}{N_m - 1}\Delta\boldsymbol{Y}_{\boldsymbol{t}}\Delta\boldsymbol{Y}_{\boldsymbol{t}}^{\top}\boldsymbol{H}_{\boldsymbol{t}}^{\top}\left(\frac{1}{N_m - 1}\boldsymbol{H}_{\boldsymbol{t}}\Delta\boldsymbol{Y}_{\boldsymbol{t}}\Delta\boldsymbol{Y}_{\boldsymbol{t}}^{\top}\boldsymbol{H}_{\boldsymbol{t}}^{\top} + \boldsymbol{R}_{\boldsymbol{t}}\right)^{-1} \tag{12}$$

where $\boldsymbol{R_t}$ was a *s* by *s* observation error covariance matrix. If two stream segments, *a* and *b*, were predicted in the forecasting phase, $\boldsymbol{R_t}$ would be expressed as:

$$\boldsymbol{R_t} = \begin{bmatrix} Variance\ z_t^a & 0 \\ 0 & Variance\ z_t^b \end{bmatrix} \tag{13}$$

where *Variance* was the estimated variance around observations of stream temperature in each stream segment at time *t*. Variance of maximum temperature observations was set to 0.25 C for all observation times and locations based on reported error in thermistors and temperature variation within stream segments when there were multiple sampling locations. More analyses are needed to determine if observation error varies significantly by location, day-of-year, or stream conditions (e.g. streamflow).

$\boldsymbol{\Delta Y_t}$ in equation 14 was an [*s* + *s* x *u*] by N_m matrix of all ensemble deviations from the average of the estimated states at time *t* ($\boldsymbol{\bar{y}_t}$), expressed as:

$$\Delta \boldsymbol{Y_t} = \left[\Delta \boldsymbol{y_{1,t}} \dots \Delta \boldsymbol{y_{m,t}} \dots \Delta \boldsymbol{y_{N_m,t}}\right] \tag{14}$$

where the *m*th column of ΔY_t was:

$$\Delta \boldsymbol{y_{m,t}} = \hat{\mathrm{y}}_{\boldsymbol{m,t}} - \boldsymbol{\bar{y}_t} \tag{15}$$

After states were updated using equation 10, the *c* states of the LSTM were set to the updated states from $\boldsymbol{Y^u_{m,t}}$, and we then proceeded to the next time step to make predictions as time *t*+1. We did not update the LSTM *h* states because maximum temperature and *c* states were updated and the *h* state is calculated from the updated *c* state.

Model training

We trained separate LSTM models on five management-relevant and well-monitored segments within the Delaware River Basin. All five stream segments are downstream from reservoirs ranging from 14.6 km to 70.1 km downstream (Figure 1). Each model was first pre-trained for 50 epochs at a learning rate of 0.05 with data from a single segment from 1985 to 2020, using the pre-training dataset as the target features and the historical drivers as the input features. Next, pre-trained model weights and biases were fine-tuned with observations of daily maximum temperature for each stream segment, for 350 epochs, at a learning rate of 0.05, using the same historical drivers from 1985-05-01 to 2021-04-14. We used 6 hidden units and recurrent and elemental dropout rates of 0.4 for both the pre-train and fine-tune phases. The model hyperparameters (e.g. number of epochs, learning rates, hidden units, dropout rates) were tuned manually to achieve reasonable model performance. Although we did not perform a thorough hyperparameter search, we found these hyperparameters to perform well for our DL forecasting models. We used TensorFlow v2.5.0 (TensorFlow Developers, 2021) to train and forecast with the LSTM models.

An ensemble of LSTM instances is required in the forecasting phase not just for uncertainty reporting but also for the data assimilation routine described above. We used 31 identical batches for each stream segment during the training phases, corresponding to the 31 ensemble members from GEFS meteorological drivers. The ending LSTM states from the fine-tune training phase were used to initialize the LSTM states during the forecasting phase.

Model forecasts

At each forecast issue time step, we made predictions 7 days into the future using the starting conditions of the previous time step's LSTM model (i.e. stream temperature, hidden, and cell states). We made predictions using trained LSTM models with data assimilation (DL-DA) and without data assimilation (DL) as well as a deterministic persistence forecast as our baseline model (Table 1). The persistence model simply forecasts the same maximum water temperature that was observed yesterday for all 7 days that follow. The DL model forecasted maximum water temperature 7 days into the future using the drivers described in Table 1. And for the DL-DA model, if there were observations available at a given time step, we assimilated the observations into the LSTM model as described in equations 10-15 and updated the stream temperature estimates and LSTM cell states (Figure 2). The DL-DA model for the next forecast issue date was initialized with the updated states and was used to make predictions 7 days into the future.

We evaluated forecasts generated from 2021-04-16 to 2021-07-16 because that was the extent of the GEFS archive that we had available. Our LSTM models used the ending states from the fine-tune training phase (fine-tune training ended on 2021-04-14) to initialize the hidden and cell states during the forecasting phase. The DL and DL-DA models incorporated three different sources of uncertainty via the ensemble predictions: driver uncertainty (e.g. GEFS ensembles), DL model uncertainty (e.g. MCD), and initial condition uncertainty (e.g. initial hidden and cell states and yesterday's maximum temperature predictions). Each DL and DL-DA model had a total of 3100 ensemble members where each of the 31 GEFS ensembles were repeated 100 times and used as batch inputs to the DL and DL-DA models. We repeated the ensemble members 100 times to produce a distribution of model predictions for each GEFS ensemble using MCD. We produced 100 predictions for each GEFS ensemble to balance the representativeness of the prediction distribution and computational speed and storage.

All model training was conducted on USGS Advance Research Computing resources (USGS Tallgrass; U.S. Geological Survey n.d.) and the operational forecasts were generated using Amazon Elastic Compute Cloud instances. Operational forecasts were run each day immediately following a scheduled observation data pull that occurred at 9:00 AM EDT. Forecasts were summarized to the average of the ensemble predictions, 90% confidence intervals (CI) of the ensembles, and the probability of exceeding 23.9°C (75°F) over the next 7 days for each of the sites of interest, and this summarized forecast output could be sent to the reservoir managers to aid in thermal release decision making (Table 2).

Table 2. *Example of summarized forecast output that can be delivered daily to the New York City reservoir managers.*

7-day water temperature forecast for Delaware River Basin, issued on 2021-06-29, using conservation release + 0cfs as the release volume.

This information is preliminary or provisional and is subject to revision. It is being provided to meet the need for timely best science. The information has not received final approval by the U.S. Geological Survey (USGS) and is provided on the condition that neither the USGS nor the U.S. Government shall be held liable for any damages resulting from the authorized or unauthorized use of the information.

	EBDR @ Harvard	**WBDR @ Hale Eddy**	**WBDR @ Hancock**	**DR @ Lordville**	**NR @ Bridgeville**
Date	***Forecasted maximum water temperature (deg F), with 90% confidence interval***				
Tuesday, June 29	71.1 (68.7-73.0)	59.4 (57.2-61.3)	64.6 (62.6-66.4)	73.9 (71.2-76.1)	72.3 (70.0-73.9)
Wednesday, June 30	70.7 (67.8-73.2)	59.0 (56.5-61.3)	64.8 (62.2-67.1)	73.9 (70.9-76.6)	71.8 (69.1-73.8)
Thursday, July 01	68.2 (64.4-72.0)	56.7 (53.8-59.5)	63.1 (59.9-66.0)	71.4 (67.8-75.0)	67.8 (63.9-71.8)
Friday, July 02	67.3 (62.8-71.2)	57.0 (53.8-60.3)	62.8 (59.4-65.8)	70.3 (65.5-74.3)	66.7 (61.9-71.1)
Saturday, July 03	66.7 (62.4-70.9)	57.6 (54.1-60.6)	62.6 (59.4-65.7)	69.4 (65.1-73.6)	66.2 (61.7-70.7)
Sunday, July 04	66.7 (62.4-70.7)	57.9 (54.9-60.8)	62.8 (59.5-65.8)	69.1 (64.9-73.6)	67.1 (62.6-71.2)
Monday, July 05	66.9 (62.6-70.9)	58.3 (55.2-61.2)	63.0 (60.1-66.0)	69.3 (64.9-73.6)	67.6 (63.1-71.4)
Tuesday, July 06	67.1 (63.0-70.9)	58.5 (55.4-61.2)	63.3 (60.3-66.4)	69.8 (65.5-73.8)	68.5 (64.6-71.8)
Date	***Probability of exceeding 75 degrees F***				
Tuesday, June 29	0	0	0	0.24	0
Wednesday, June 30	0	0	0	0.32	0
Thursday, July 01	0	0	0	0.05	0
Friday, July 02	0	0	0	0.02	0
Saturday, July 03	0	0	0	0.01	0
Sunday, July 04	0	0	0	0.01	0
Monday, July 05	0	0	0	0.01	0
Tuesday, July 06	0	0	0	0.01	0

Model evaluation

We evaluated model forecast performance with root mean squared error (RMSE), continuous ranked probability score (CRPS; Thomas et al. 2021), and bias by comparing valid date predictions to observations of maximum temperature that occurred on the same dates. Bias and RMSE reflect accuracy of the average of the ensembles relative to the observed maximum temperature. We also evaluated the distribution of ensemble predictions using CRPS, which measures both the accuracy and precision of a probabilistic forecast, where lower values indicate a better model. Because multiple forecasts were valid for any given day, this allowed us to analyze how model forecast accuracy changed with different lead times and how it may change across the entire forecast period.

We evaluated how well the model characterizes forecast uncertainty with reliability plots where we calculate the proportion of observations that fall within confidence intervals calculated from the ensemble predictions as in Thomas et al. (2021). A well-calibrated forecasting model would have 10% of observations within the 10% forecast confidence interval (i.e., the 45th-55th quantiles of the forecast probability distribution), 20% of observations in the 20% forecast confidence interval (the 40th-60th quantiles), and so on. If a higher or lower percentage of the observations fall within a given forecast confidence interval, then the model is considered underconfident or overconfident, respectively.

Model code used to create pre-training process-based datasets, train the DL models, and forecast with the trained DL models can be found at Zwart et al. (2021). All model drivers and predictions used in this analysis can be found at Oliver et al. (2021).

Results

Data assimilation and deep learning

Our data assimilation routine successfully updated LSTM cell states using equations 9-15. As an example, we used the Delaware River at Lordville DL-DA model to show relations between temperature predictions, LSTM cell states, and adjustment of these states after assimilating observations of daily maximum stream temperature. The sample error covariance showed that some cell states covaried more strongly with temperature than others, as cell state 2, 5, and 6 had the strongest covariance with maximum stream temperature predictions for the Lordville DL-DA model (Figure 3). Assimilating daily maximum temperature observations into the LSTM adjusted the average ensemble temperature and cell states (Figure 4). Daily maximum stream temperature predictions and cell state 2, 5, and 6 showed the greatest adjustment after assimilating daily maximum stream temperature observations for the Lordville DL-DA model.

After assimilating daily maximum stream temperature observations into the LSTM, bias in the average of the ensemble daily maximum stream temperature predictions compared to observations was reduced (Figure 5). Daily maximum stream temperature observations were only available for lead time day -1 (Figure 2), so Figure 5 represents the bias in maximum stream temperature predictions for lead time day -1 for both the DL (prior) and DL-DA (posterior) models.

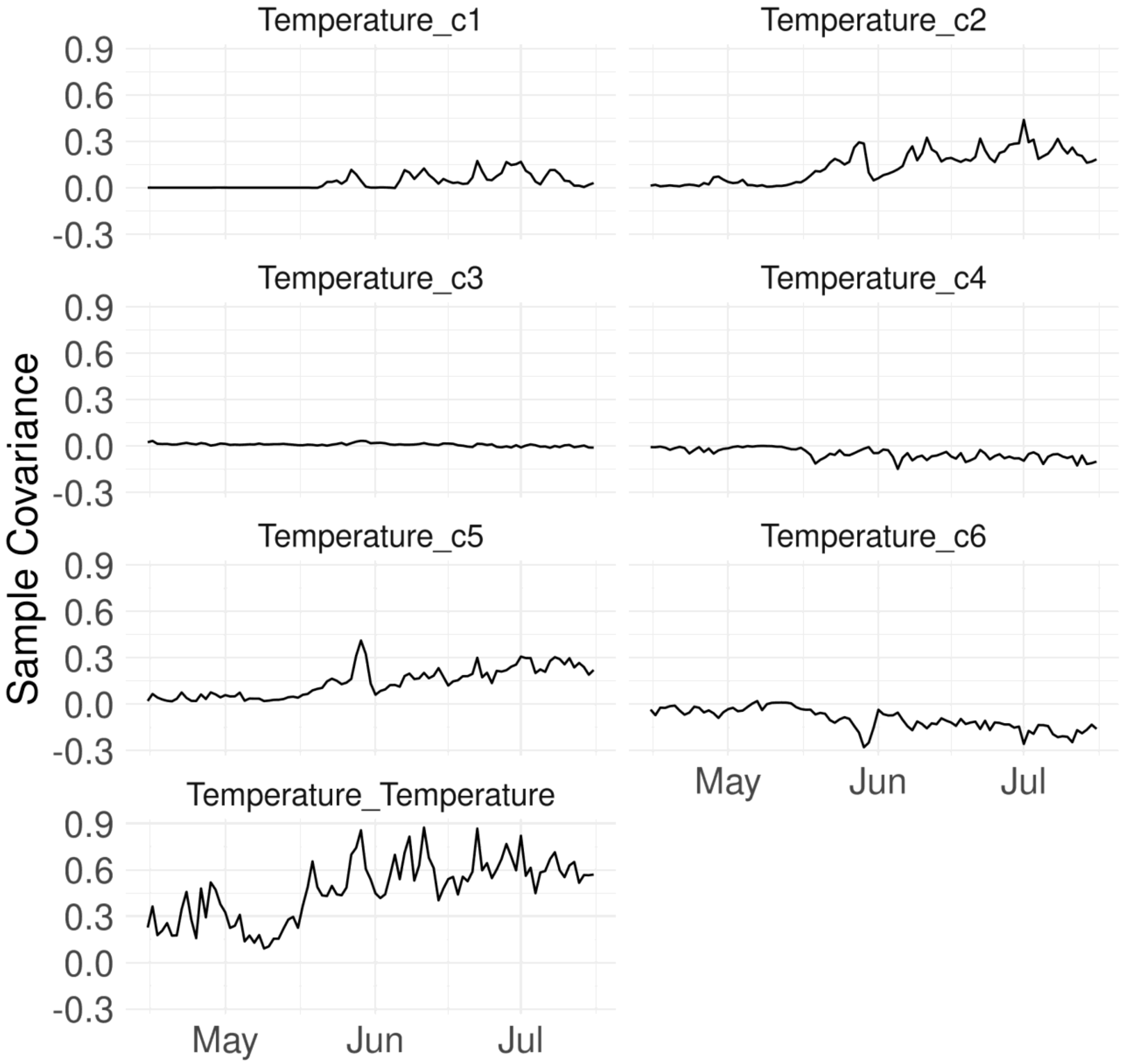

***Figure 3**. Sample covariance between daily maximum stream temperature predictions (Temperature) and LSTM cell states 1-6 (c1-c6) for the Delaware River at Lordville DL-DA model from 2021-04-15 to 2021-07-16. Sample covariance is calculated as* $\frac{1}{N_m-1}\Delta\boldsymbol{Y_t}\Delta\boldsymbol{Y_t}^{\top}$ *as shown in equation 12.*

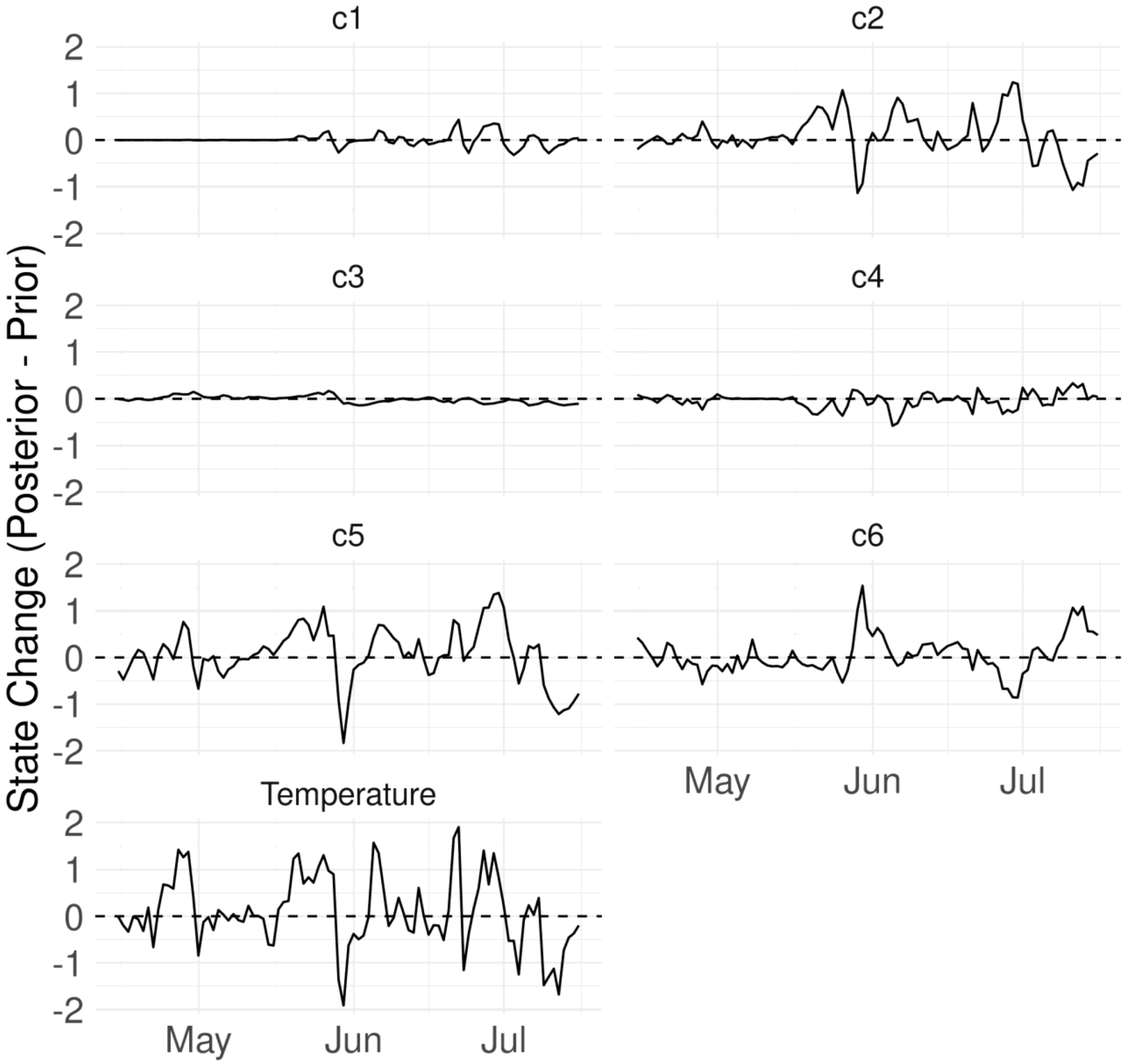

Figure 4. *Average ensemble state change for the six LSTM states (c1-c6) and the daily maximum stream temperature prediction (Temperature) for the Delaware River at Lordville DL-DA model from 2021-04-15 to 2021-07-16. The average state change is calculated as the difference between the average of the prior state distribution and the average of the posterior state distribution after assimilating daily maximum temperature observations.*

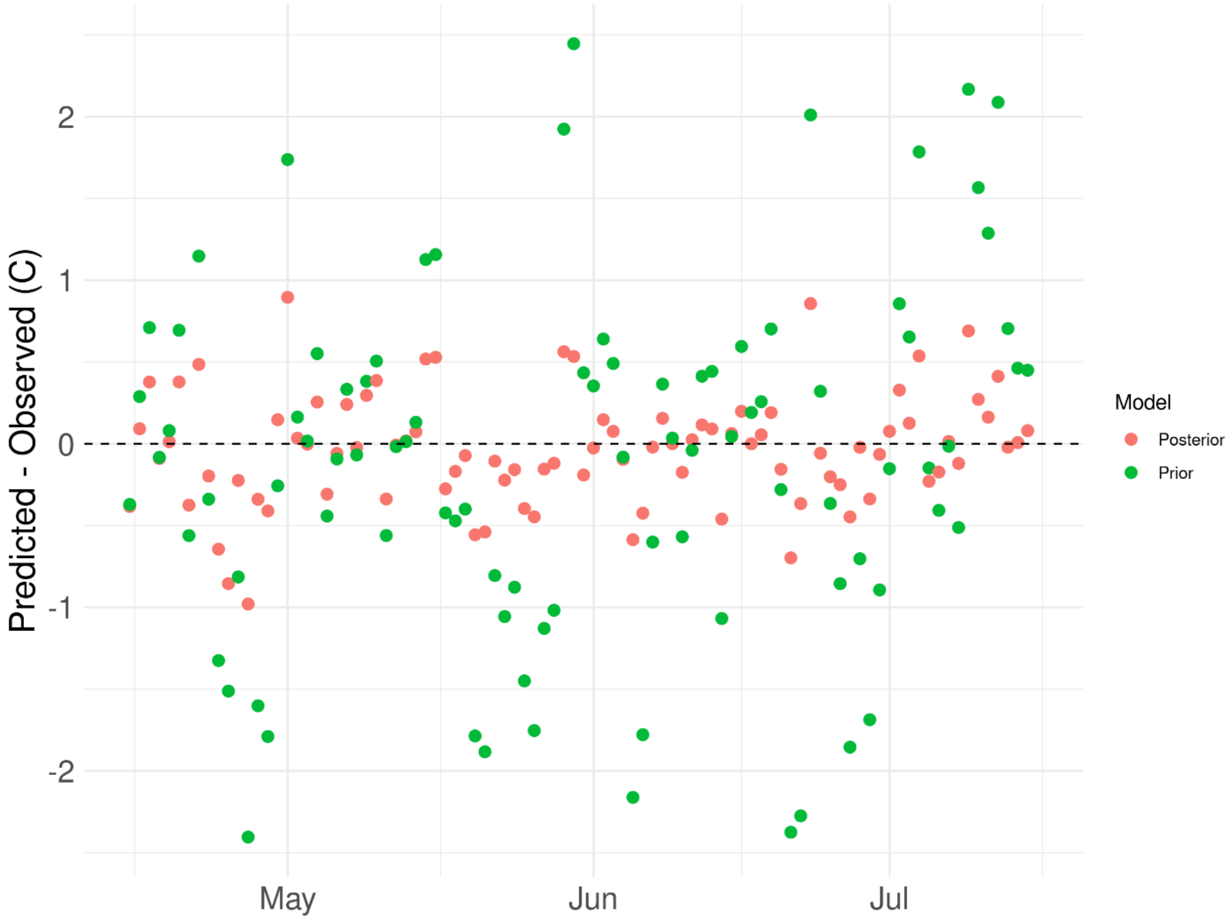

***Figure 5**. Difference between predicted daily maximum stream temperature and observed daily maximum stream temperature for Delaware River at Lordville site from 2021-04-15 to 2021-07-16 for both the average of the prior distribution and the average of the posterior distribution after assimilating daily maximum stream temperature observations.*

Model accuracy

The addition of our data assimilation algorithm (DL-DA model, Figure 6) marginally improved DL forecast performance for lead times 0 and 1 across all stream segments (7-13% lower RMSE) but had a greater increase in performance for the sites below Pepacton Reservoir (East Branch of the Delaware River [EBDR] at Harvard and the Delaware River [DR] at Lordville) and Neversink Reservoir (Neversink River [NR] at Bridgeville) reservoirs. In some cases, data assimilation reduced forecast accuracy (e.g. CRPS for West Branch of the Delaware River [WBDR] at Hale Eddy site) and increased model absolute bias; however, differences in RMSE, CRPS, and biases were minimal (>2% difference) when data assimilation reduced DL model performance.

Our models produced predictions of maximum stream temperature from 1-7 day lead times, with RMSEs ranging from 1.2 to 1.6°C across all segments for day-ahead forecasts (lead time day 1) for the DL-DA model (Figure 6). Performance of the models generally worsened as lead time increased; RMSE ranged from 1.5 to 2.2°C across segments for 7-day ahead DL-DA forecasts. Temperature at the site below the Neversink Reservoir (NR @ Bridgeville) was the hardest to predict as NR @ Bridgeville site had the highest RMSE, greatest bias (underpredicted), and highest CRPS for all lead times and both across all models. DL and DL-DA model absolute bias was within 0.2°C for all sites and lead times except for the NR @ Bridgeville site. Persistence forecast bias became more negative at longer lead times, which is expected when evaluating stream temperature forecasts issued during the spring to early summertime periods.

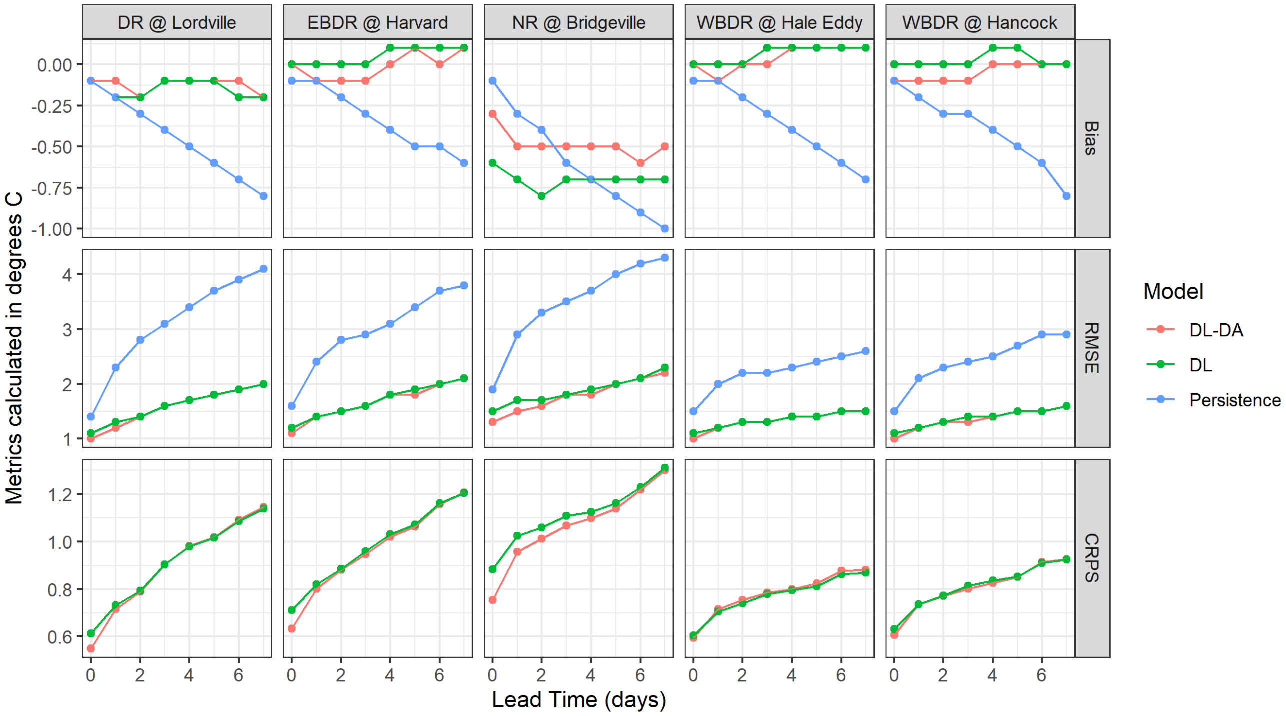

***Figure 6**. Model forecast accuracy as a function of forecast lead time for each site in the Delaware River Basin, including bias, root mean squared error (RMSE), and continuous ranked probability score (CRPS). Forecasts were produced for the Delaware River at Lordville (DR @ Lordville), East Branch of the Delaware River at Harvard (EBDR @ Harvard), Neversink River at Bridgeville (NR @ Bridgeville), West Branch of the Delaware River at Hale Eddy (WBDR @ Hale Eddy), the West Branch of the Delaware River at Hancock (WBDR @ Hancock).*

Model Reliability

Our DL and DL-DA models characterized uncertainty relatively well as 57 to 80% of observations were within 90% confidence intervals (CIs) across all sites, models, and lead times (Figure 7). Overall, there was very little difference in reliability between the DL and DL-DA models. Uncertainty estimates were mildly overconfident, with more reliable uncertainty estimates for the central 10% of the CI distribution and greater overconfidence for larger CIs. There was not a clear pattern in forecast reliability for differing lead times across sites, as lower lead times were generally more reliable for some sites (e.g. DR @ Lordville), while longer lead times were more reliable for other sites (e.g. NR @ Bridgeville).

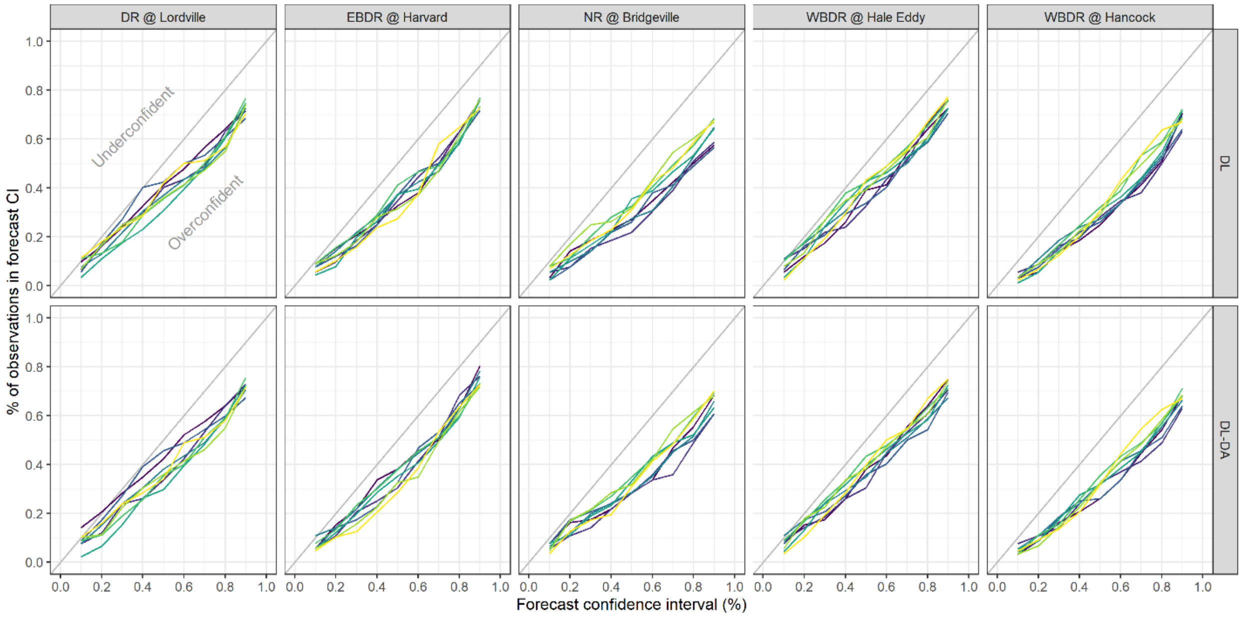

Figure 7. *Reliability plots showing the percentage of observations occurring in each of nine forecast confidence intervals, for deep learning (DL) forecasts (top row) and deep learning with data assimilation (DL-DA) forecasts (bottom row). A well-calibrated forecast model would fall along the 1:1 line. Forecasts were produced for the Delaware River at Lordville (DR @ Lordville), East Branch of the Delaware River at Harvard (EBDR @ Harvard), Neversink River at Bridgeville (NR @ Bridgeville), West Branch of the Delaware River at Hale Eddy (WBDR @ Hale Eddy), the West Branch of the Delaware River at Hancock (WBDR @ Hancock).*

Impact of Release Scenarios

Our DL-DA model predicted a decrease in stream water temperature in response to the additional 100cfs release added to lead time day 1 (Figure 8). The average decrease in stream temperature across all forecast issue times in June and July with a 1-day lead time was 0.13, 0.14, and 0.10°C at the WBDR @ Hale Eddy, WBDR @ Hancock, and DR @ Lordville sites, respectively. The effect of the simulated reservoir release on the simulated temperatures at WBDR @ Hale Eddy and Hancock was greater than that DR @ Lordville. Across all sites, the effect of the simulated release decreased at longer lead times. For nearly all lead times at the WBDR @ Hale Eddy and Hancock sites, the upper 90th percentile prediction was affected more by the simulated reservoir release compared to the average prediction and the lower 90th percentile prediction.

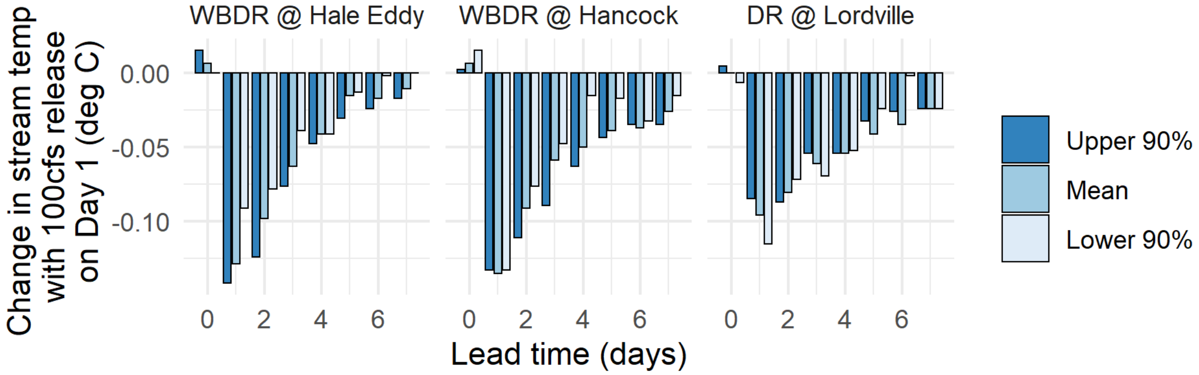

Figure 8. *Change in simulated maximum stream temperature from a simulated 100cfs release from the Cannonsville Reservoir added to lead time day 1. Data shown are from June and July and averaged across all forecast issue dates. The EBDR @ Harvard and NR @ Bridgeville sites are not shown because they are not affected by releases from the Cannonsville Reservoir.*

Discussion

Accurate and reliable forecasts of environmental variables are becoming important tools for environmental resource management (Dietze et al., 2018; Bradford et al. 2020). Using a novel integration of DL and DA, our models produced accurate predictions of maximum stream water temperature 7 days into the future for forecasts issued between 2021-04-16 and 2021-07-16, with an average RMSE of 1.5°C across all sites and forecast lead times. Our models also characterized uncertainty relatively well and can aid reservoir managers in decisions about when to release water from reservoirs to cool stream segments. Below we discuss the forecast performance and further development that could improve upon the DL-DA forecast accuracy and reliability.

Forecast accuracy

Although our models produced accurate predictions overall, there was variation in performance across sites and lead times (Figure 6). The persistence forecast performance can give insight into the predictability across sites as better performing persistence forecasts often indicated better performing DL and DL-DA model performance. For example, WBDR @ Hale Eddy and Hancock sites had the best performing persistence, DL, and DL-DA forecasts at longer lead times, indicating that there is likely stronger autocorrelation in maximum stream temperature at these sites and higher predictability (Figure 3). Stream temperature at these sites are heavily influenced by the upstream Cannonsville Reservoir and water released from the reservoir likely mutes variability in maximum stream temperature thereby increasing autocorrelation. This contrasts with the NR @ Bridgeville site which generally had the lowest forecast performance for the persistence, DL, and DL-DA models across all lead times. The NR @ Bridgeville DL model was potentially missing important drivers that influence maximum stream temperature such as streamflow or precipitation. We did not model reservoir temperature in the Neversink Reservoir above Bridgeville, and the lack of a pre-trainer that simulated reservoir outlet dynamics may have partially accounted for decreased performance at this site. To improve upon the accuracy of DL model forecasts for these sites, DL models could be trained across multiple sites (Kratzert et al. 2019b), additional upstream information or meteorological variables could be added as drivers (Rahmani et al. 2020), or the DL model structure could be modified to represent network connections across stream segments (Jia et al. 2021).

Data assimilation and deep learning

We found that combining data assimilation with our DL models modestly improved forecast performance of maximum stream temperature, typically at 0- and 1-day lead times, compared to our DL model without data assimilation. Data assimilation is heavily relied upon in forecasting applications to adjust model states, parameters, and drivers prior to issuing forecasts, and there are increasingly more examples of assimilating data into DL models to make improved predictions. For example, Brajard et al. (2020) use an iterative DL and data assimilation algorithm to emulate the Lorenz 96 model using sparse and noisy observations, which can be a challenging task for DL models alone, and Fang and Shen (2020) show that a data integration kernel within a DL model improves near-term forecasts of soil moisture. Given these past successes for improving DL predictions with data assimilation, we might expect our DL-DA model to show even more improvement beyond our DL model without data assimilation. However, the modest improvement is likely due to our base DL model still having access to the same observation information as the DL-DA model because yesterday's maximum temperature observation was used as a model driver for both the DL and DL-DA models. Additionally, loss of information occurs using any data assimilation algorithm (Nearing et al. 2018) and the choice of the data assimilation algorithm will dictate how efficiently the algorithm combines these pieces of information together. Given these losses of information from data assimilation algorithms with rigid assumptions, it may be beneficial to allow the DL model itself decide how to use the new observation information; however, more research is needed to assess which data assimilation algorithms optimally combine new observations with DL model predictions to improve forecast performance.

Forecast uncertainty

Our DL-DA model characterized forecast uncertainty well; however, the model tended to be overconfident in predictions for the time period we analyzed. The overconfidence is likely due to overfitting models to the training dataset, which is a common problem in all types of modeling, especially machine learning. To improve upon the forecast uncertainty estimates, we may want to train global DL models on many stream segments and fine-tune to individual segments, add in noise regularization to the drivers during training, and / or increase the dropout rate for the recurrent and input elements during model training. Additionally, Klotz et al. (2021) show that mixture density networks have better uncertainty characterization compared to MCD for streamflow predictions, indicating that adoption of these relatively newer methods may be promising for improving DL forecast reliability.

Reservoir release scenarios

Some forecast products can trigger decisions that alter the conditions being forecasted; in our use case, a forecast that predicts water temperature will exceed 23.9°C (75°F) in the future could trigger a manger to call for larger reservoirs releases that would cool downstream waters to maintain coolwater fish habitat. Generating a forecast with feedbacks that can be exposed to the decision maker can make the forecasts more actionable. Our implementation included two water release scenarios, which provided a range of expected outcomes for taking no action (conservation releases +0cfs thermal bank release) and alternatively, issuing a single-day preventative action (conservation releases +100cfs release; see Figure 5) designed to keep future downstream water temperatures from exceeding a biologically relevant temperature threshold. We observed a decrease in stream temperature following the reservoir release scenario, with the DR @ Lordville site having the smallest response, which was expected because DR @ Lordville was the farthest downstream from the Cannonsville Reservoir of the three sites. Although we observed an expected decrease in stream water temperature following the +100cfs release scenario, the resulting average decrease was small for the three segments downstream from the Cannonsville Reservoir (decrease ~0.1°C). Currently, the model does not explicitly have information that would help it distinguish between increases in release volumes that are coming from the surface of the reservoir (through the spillway) versus the bottom of the reservoir (via conservation or directed releases), nor is it exposed to flow changes related to precipitation events. We speculate that adding in stream discharge and/or precipitation as an additional model driver may help the DL model learn about the effects of reservoir releases under various release conditions. Additionally, we could expose the DL model to more pre-training scenarios that could help the model learn about the effect of reservoir releases on downstream temperature, potentially increasing the effect of reservoir release on changes in stream temperature.

Future efforts could extend this simple +0cfs/+100cfs case by exposing a greater variety of scenarios to reservoir release decision makers, including additional release volumes and their future timing (e.g., beyond the day-of-issue). Alternatively, the complete modeling system could be provided to the end-users where model inputs could be fully controlled by the decision makers. The combination of real-time data and modern deep learning modeling advances described here can provide timely and accurate information for critical water resources decisions.

Summary

We demonstrate the utility of combining data assimilation with DL models for forecasting management-relevant environmental variables. Our DL-DA model produced accurate and reasonably reliable forecasts of maximum stream temperature 7 days into the future. Despite the reliability and accuracy of the forecasts, future improvements could include increasing the complexity of the underlying models or the modes of DA, in addition to providing sub-daily inputs to the model that could help better resolve daily maximum temperatures. Given the flexibility of DL models, we expect future extensions and improvements on this type of framework could be used for many types of environmental forecasting applications.

Acknowledgements

All model training was run on USGS High Performance Computing. We thank Grey Nearing for valuable input on the forecasting model design decisions. We thank Tadgh Moore for sharing his experience and insights on reservoir modelling. We thank Reza Abdi and James McCreight for valuable feedback when reviewing earlier drafts of this manuscript. Any use of trade, firm, or product names is for descriptive purposes only and does not imply endorsement by the U.S. Government.

References

Abatzoglou, J.T., 2013. Development of gridded surface meteorological data for ecological applications and modelling. Int. J. Climatol. 33, 121–131. https://doi.org/10.1002/joc.3413

Abdi, R., Endreny, T., Nowak, D., 2020. A model to integrate urban river thermal cooling in river restoration. J. Environ. Manage. 258, 110023. https://doi.org/10.1016/j.jenvman.2019.110023

Block, P.J., Souza Filho, F.A., Sun, L., Kwon, H.-H., 2009. A streamflow forecasting framework using multiple climate and hydrological models. JAWRA J. Am. Water Resour. Assoc. 45, 828–843. https://doi.org/10.1111/j.1752-1688.2009.00327.x

Bock, A., Viger, R., 2014. GIS features of the geospatial fabric for National Hydrologic Modeling. https://doi.org/10.5066/F7542KMD

Bradford, J.B., Weltzin, J., Mccormick, M., Baron, J., Bowen, Z., Bristol, S., Carlisle, D., Crimmins, T., Cross, P., DeVivo, J., Dietze, M., Freeman, M., Goldberg, J., Hooten, M., Hsu, L., Jenni, K., Keisman, J.L., Kennen, J., Lee, K., Lesmes, D., Loftin, K., Miller, B.W., Murdoch, P.S., Newman, J., Prentice, K.L., Rangwala, I., Read, J., Sieracki, J., Sofaer, H., Thur, S., Toevs, G., Werner, F., White, C.L., White, T., Wiltermuth, M., 2020. Ecological forecasting—21st century science for 21st century management. U.S. Geological Survey Open-File Report 2020–1073. https://doi.org/10.3133/ofr20201073

Brajard, J., Carrassi, A., Bocquet, M., Bertino, L., 2020. Combining data assimilation and machine learning to emulate a dynamical model from sparse and noisy observations: A case study with the Lorenz 96 model. J. Comput. Sci. 44, 101171. https://doi.org/10.1016/j.jocs.2020.101171

Clark, J.S., 2001. Ecological forecasts: An emerging imperative. Science 293, 657–660. https://doi.org/10.1126/science.293.5530.657

Dietze, M.C., 2017. Prediction in ecology: a first-principles framework. Ecol. Appl. 27, 2048–2060. https://doi.org/10.1002/eap.1589

Dietze, M.C., Fox, A., Beck-Johnson, L.M., Betancourt, J.L., Hooten, M.B., Jarnevich, C.S., Keitt, T.H., Kenney, M.A., Laney, C.M., Larsen, L.G. and Loescher, H.W., 2018. Iterative near-term ecological forecasting: Needs, opportunities, and challenges. Proceedings of the National Academy of Sciences, 115, 1424-1432. https://doi.org/10.1073/pnas.1710231115

Dietze, M.C., Lebauer, D.S., Kooper, R., 2013. On improving the communication between models and data. Plant Cell Environ. 36, 1575–1585. https://doi.org/10.1111/pce.12043

Evensen, G., 1994. Sequential data assimilation with a nonlinear quasi-geostrophic model using Monte Carlo methods to forecast error statistics. J. Geophys. Res. 99, 10143. https://doi.org/10.1029/94JC00572

Fang, K., Shen, C., 2020. Near-real-time forecast of satellite-based soil moisture using long short-term memory with an adaptive data integration kernel. J. Hydrometeorol. 21, 399–413. https://doi.org/10.1175/JHM-D-19-0169.1

Gal, Y., Ghahramani, Z., 2016. Dropout as a bayesian approximation: Representing model uncertainty in deep learning, in: Proceedings of The 33rd International Conference on Machine Learning, Proceedings of Machine Learning Research. PMLR, pp. 1050–1059.

Hansen, C., Shafiei Shiva, J., McDonald, S., Nabors, A., 2019. Assessing retrospective National Water Model streamflow with respect to droughts and low flows in the Colorado River Basin. JAWRA J. Am. Water Resour. Assoc. 55, 964–975. https://doi.org/10.1111/1752-1688.12784

Hipsey, M.R., Bruce, L.C., Boon, C., Busch, B., Carey, C.C., Hamilton, D.P., Hanson, P.C., Read, J.S., de Sousa, E., Weber, M., Winslow, L.A., 2019. A General Lake Model (GLM 3.0) for linking with high-frequency sensor data from the Global Lake Ecological Observatory Network (GLEON). Geosci. Model Dev. 12, 473–523. https://doi.org/10.5194/gmd-12-473-2019

Hirsch, R.M., Fisher, G.T., 2014. Past, present, and future of water data delivery from the U.S. Geological Survey. J. Contemp. Water Res. Educ. 153, 4–15. https://doi.org/10.1111/j.1936-704X.2014.03175.x

Jain, A., Kumar Varshney, A., Chandra Joshi, U., 2001. Short-term water demand forecast modelling at IIT Kanpur using Artificial Neural Networks. Water Resour. Manag. 15, 299–321. https://doi.org/10.1023/A:1014415503476

Jia, X., Zwart, J., Sadler, J., Appling, A., Oliver, S. K., Markstrom, S. L., Willard, J., Xu, S., Steinbach, M., Kumar, V., 2021. Physics-guided Recurrent Graph Model for predicting flow and temperature in river networks. Proc. 2021 SIAM Int. Conf. Data Min. SDM 612–620.

Klotz, D., Kratzert, F., Gauch, M., Keefe Sampson, A., Brandstetter, J., Klambauer, G., Hochreiter, S., Nearing, G., 2021. Uncertainty estimation with deep learning for rainfall-runoff modelling. Hydrol. Earth Syst. Sci. Discuss. 1–32. https://doi.org/10.5194/hess-2021-154

Kratzert, F., Herrnegger, M., Klotz, D., Hochreiter, S., Klambauer, G., 2019a. NeuralHydrology -- Interpreting LSTMs in hydrology. ArXiv190307903 Phys. Stat 11700, 347–362. https://doi.org/10.1007/978-3-030-28954-6_19

Kratzert, F., Klotz, D., Shalev, G., Klambauer, G., Hochreiter, S. and Nearing, G., 2019b. Towards learning universal, regional, and local hydrological behaviors via machine learning applied to large-sample datasets. Hydrol. Earth Syst. Sci., 23(12), 5089-5110.

Kratzert, F., Klotz, D., Brenner, C., Schulz, K., Herrnegger, M., 2018. Rainfall–runoff modelling using Long Short-Term Memory (LSTM) networks. Hydrol. Earth Syst. Sci. 22, 6005–6022. https://doi.org/10.5194/hess-22-6005-2018

Lee, S., Lee, D., 2018. Improved prediction of harmful algal blooms in four major South Korea's rivers using deep learning models. Int. J. Environ. Res. Public. Health 15, 1322. https://doi.org/10.3390/ijerph15071322

Markstrom, S. L., 2012. P2S—Coupled simulation with the Precipitation-Runoff Modeling System (PRMS) and the Stream Temperature Network (SNTemp) Models. U.S. Geological Survey Open-File Report 2012-1116. https://doi.org/10.3133/ofr20121116

Massoud, E.C., Huisman, J., Benincà, E., Dietze, M.C., Bouten, W., Vrugt, J.A., 2018. Probing the limits of predictability: data assimilation of chaotic dynamics in complex food webs. Ecol. Lett. 21, 93–103. https://doi.org/10.1111/ele.12876

Matos, J.S., de Sousa, E.R., 1996. Prediction of dissolved oxygen concentration along sanitary sewers. Water Sci. Technol., Water Quality International '96 Part 3: Modelling of Activated Sludge Processes; Microorganisms in Activated Sludge and Biofilm Processes; Anareobic Biological Treatment; Biofouling 34, 525–532. https://doi.org/10.1016/0273-1223(96)00688-9

Nearing, G., Yatheendradas, S., Crow, W., Zhan, X., Liu, J., Chen, F., 2018. The efficiency of data assimilation. Water Resour. Res. 54, 6374–6392. https://doi.org/10.1029/2017WR020991

Nystrom, E.A., 2018. Bathymetry of Ashokan, Cannonsville, Neversink, Pepacton, Rondout, and Schoharie Reservoirs, New York. U.S. Geological Survey Scientific Investigations Report 2017–5064. https://doi.org/10.3133/sir20175064

Oliver, S., Appling, A., Atshan, R., Watkins, W., Sadler, J., Corson-Dosch, H., Zwart, J., Read, J., 2021. Data release: Predicting water temperature in the Delaware River Basin. U.S. Geological Survey data release. https://doi.org/10.5066/P9GD8I7A

Rahmani, F., Lawson, K., Ouyang, W., Appling, A., Oliver, S., Shen, C., 2020. Exploring the exceptional performance of a deep learning stream temperature model and the value of streamflow data. Environ. Res. Lett. https://doi.org/10.1088/1748-9326/abd501

Read, E.K., Carr, L., De Cicco, L., Dugan, H.A., Hanson, P.C., Hart, J.A., Kreft, J., Read, J.S., Winslow, L.A., 2017. Water quality data for national-scale aquatic research: The Water Quality Portal. Water Resour. Res. 53, 1735–1745. https://doi.org/10.1002/2016WR019993

Read, J.S., Jia, X., Willard, J., Appling, A.P., Zwart, J.A., Oliver, S.K., Karpatne, A., Hansen, G.J., Hanson, P.C., Watkins, W., Steinbach, M., 2019. Process-guided deep learning predictions of lake water temperature. Water Resour. Res. 55, 9173-9190. https://doi.org/10.1029/2019WR024922

Reichle, R.H., 2008. Data assimilation methods in the Earth sciences. Adv. Water Resour. 31, 1411–1418. https://doi.org/10.1016/j.advwatres.2008.01.001

Rumelhart, David E., Geoffrey E. Hinton, and Ronald J. Williams. 1986. Learning representations by back-propagating errors. Nature 323, no. 6088: 533-536.

Sanders, M. J., Markstrom, S. L., Regan, R. S., Atkinson, R. D., 2017. Documentation of a daily mean stream temperature module—An enhancement to the Precipitation-Runoff Modeling System, U.S. Geological Survey Techniques and Methods 6-D4. https://doi.org/10.3133/tm6D4

Shen, C., 2018. A transdisciplinary review of deep learning research and its relevance for water resources scientists. Water Resour. Res. 54, 8558–8593. https://doi.org/10.1029/2018WR022643

TensorFlow Developers. (2021). TensorFlow (v2.5.0). Zenodo. https://doi.org/10.5281/zenodo.4758419

Thomas, R.Q., Figueiredo, R.J., Daneshmand, V., Bookout, B.J., Puckett, L.K., Carey, C.C., 2021. A near-term iterative forecasting system successfully predicts reservoir hydrodynamics and partitions uncertainty in real time. Water Resour. Res. 56. https://doi.org/10.1029/2019WR026138

Turner, S.W.D., Xu, W., Voisin, N., 2020. Inferred inflow forecast horizons guiding reservoir release decisions across the United States. Hydrol. Earth Syst. Sci. 24, 1275–1291. https://doi.org/10.5194/hess-24-1275-2020

U.S. Geological Survey, 2021, National Water Information System data available on the World Wide Web (USGS Water Data for the Nation), accessed [July 17 10, 2021], at https://doi.org/10.5066/F7P55KJN

U.S. Geological Survey Advanced Research Computing, n.d. USGS Tallgrass Supercomputer: U.S. Geological Survey, https://doi.org/10.5066/P9XE7ROJ

Viel, C., Beaulant, A.-L., Soubeyroux, J.-M., Céron, J.-P., 2016. How seasonal forecast could help a decision maker: an example of climate service for water resource management. Adv. Sci. Res. 13, 51–55. https://doi.org/10.5194/asr-13-51-2016

Viger, R.J., 2014. Preliminary spatial parameters for PRMS based on the Geospatial Fabric, NLCD2001, and SSURGO. https://doi.org/10.5066/F7WM1BF7

Vörösmarty, C.J., 2000. Global water resources: Vulnerability from climate change and population growth. Science 289, 284–288. https://doi.org/10.1126/science.289.5477.284

Williamson, T.N., Lant, J.G., Claggett, P.R., Nystrom, E.A., Milly, P.C.D., Nelson, H.L., Hoffman, S.A., Colarullo, S.J., Fischer, J.M., 2015. Summary of hydrologic modeling for the Delaware River Basin using the Water Availability Tool for Environmental Resources (WATER) (USGS Numbered Series No. 2015–5143), Scientific Investigations Report. U.S. Geological Survey, Reston, VA.

Xiang, Z., Demir, I., 2020. Distributed long-term hourly streamflow predictions using deep learning – A case study for State of Iowa. Environ. Model. Softw. 131, 104761. https://doi.org/10.1016/j.envsoft.2020.104761

Zwart, J.A., Oliver, S.K., Watkins, W.D., Sadler, J., Appling, A.P., Corson-Dosch H.R., Jia, X., Kumar, V., Read, J.S. 2021. Source code: Near-term forecasts of stream temperature using process-guided deep learning and data assimilation (version 0.9.0). Zenodo. http://doi.org/10.5281/zenodo.5164910